Karlsruhe Institute of Technology

Fakultät für Physik
Physikalisches Institut

Influence of Coupling Strength on Transmission Properties of a rf-SQUID Transmission Line

Einfluss der Kopplungsstärke auf die Transmissionseigenschaften einer rf-SQUID Transmissionsleitung

Bachelorarbeit

von

Michael Wolfstädter

Erstgutachter: Prof. Dr. Alexey V. Ustinov
Betreuender Mitarbeiter: Susanne Butz

Contents

Introduction

In this work the transmission properties of **S**uperconducting **QU**antum **I**nterference **D**evices (SQUIDs) in a coplanar transmission line are investigated. We examined the effect of the coupling between rf-SQUIDs. An rf-SQUIDs consists of a superconducting ring containing a single Josephson junction.
A current in one SQUID induces a current in neighboring SQUIDs. The extent of the induced current in the neighboring SQUIDs depends, among other factors, on the distance between the SQUIDs. We measured the effect of this magnetoinductive coupling on the transmission of microwaves through a coplanar transmission line along a linear array of rf-SQUIDs.
Via this method it is tested if a certain measure depends on the periodicity of the SQUIDs, too. The measure of interest is the power range within which the transmission depends on the externally applied flux.

Outline
In section 1 the theoretical background for our experiments is explained. This includes the basic principles of superconductivity. The Josephson relations and the physics of rf-SQUIDs is explained as well as a derivation of the coupling strength between SQUIDs in a one dimensional array.
Section 2 concentrates on describing the measurement setup and the measurement procedure. The results of our measurements are presented in section 3 as well as the general method of analysis of our measured data. For this purpose the concept of mutual inductance and coupling coefficient is discussed. Calculations for comparing the currents induced in a SQUID by the coplanar transmission line or another SQUID are shown. After that the influence of microwave properties on transmission is explained and an interesting property of SQUID behavior - the "2-dips-per-Φ_0 phenomenon" - is found and explained. Then the results are analyzed in different ways and interpreted.
A conclusion and an outlook are presented in section 4.

1 Basics

1.1 Superconductivity

Superconductivity describes a state in which two electrons (i.e. fermions) interact via phonons and form a Cooper pair (i.e. bosons). All Cooper pairs within one superconductor are described by a single wavefunction

$$\Psi(\vec{r}) = \sqrt{\frac{n_s}{2}} e^{i\Theta} \tag{1}$$

with n_s being the number density of Cooper pairs and Θ being the phase [1].
Due to the energy gap in the band structure of superconductors there are no states to scatter to. As there is no scattering the flow of Cooper pairs is dissipationless [1].
There are certain conditions to be met for electrons to go into the superconductive state. Superconductivity occurs only below a critical Temperature T_c which is in the single digit range of the Kelvin temperature scale for most superconductive materials and is correlated with the size of the energy gap. Furthermore a critical magnetic field H_{cm} may not be exceeded. The value of H_{cm} depends on the Temperature:

$$H_{cm}(T) = H_{cm}(0) \cdot \left(1 - \frac{T}{T_c}^2\right). \tag{2}$$

Magnetic Flux Quantization
In a superconducting loop the common wavefunction of all Cooper pairs interferes with itself after each full loop. Thus the wavefunction has to be single valued after each phase change of 2π. Therefore only integral multiples of the flux quantum $\Phi_0 = \frac{h}{2e} = 2.07 \cdot 10^{-15}$Wb can penetrate the loop [1].

1.2 Josephson Effects and RCSJ-Model

The DC- as well as the AC-Josephson Effect occur when two superconductors are connected through a weak link [1]. We used so called Josephson junctions as weak links. These consist of a thin isolating layer.
Across the Josephson junction the wavefunctions of both superconductors overlap as shown in figure 1. Between the wavefunctions there is a phase difference $\varphi = \theta_2 - \theta_1$.

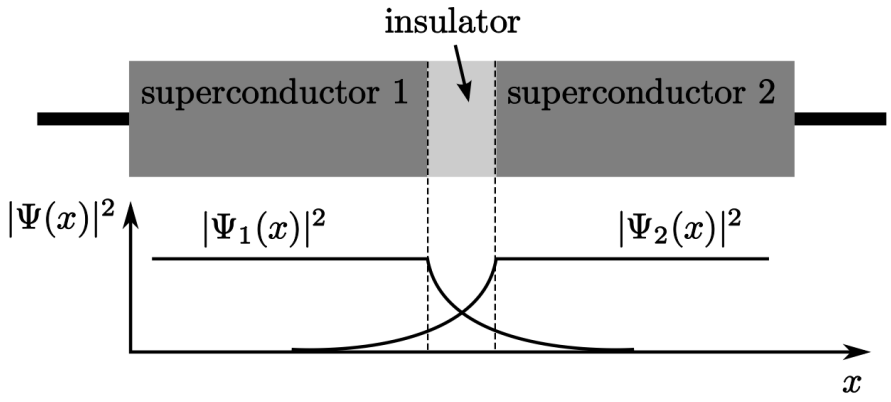

Figure 1: Overlapping wavefunctions of connected superconductors [2].

Equations (3) and (4) show the Josephson relations.
For small currents $I_s < I_c$ the DC-Josephson relation (3) describes the superconducting DC-current I_s that can flow through the junction depending on the phase difference φ. Its maximal value is I_c. This can be seen from another perspective: with a fixed DC-current applied the phase difference will adjust itself according to equation (3).

$$I_s = I_c \cdot \sin(\varphi) \tag{3}$$

$$\hbar \frac{\partial \varphi}{\partial t} = 2eV \tag{4}$$

The AC-Josephson relation (4) describes the relation between the voltage V and the time-dependent change in the phase φ. If the total current exceeds I_c then a voltage V appears across the junction. As the supercurrent, according to equation (3), cannot exceed I_c there must be a normal current I_n consisting of quasiparticles flowing in parallel to the supercurrent in this regime.

A way to describe the occurrence of the mentioned normal current and therefore the occurring resistance is the **R**esistively and **C**apacitively **S**hunted **J**unction model (RCSJ model) [3] in which a capacitance and a resistor are in parallel to the Josephson junction as shown in figure 2. The capacity C describes the capacitive behavior of the junction, the resistance R the resistive behavior.

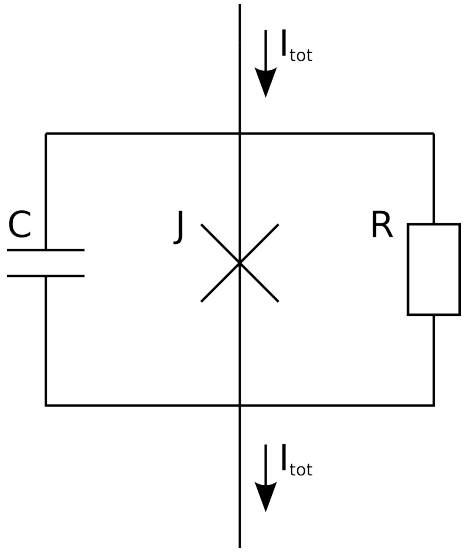

Figure 2: RCSJ circuit diagram.

According to Kirchhoff's law the total current can be calculated as follows:

$$I_{tot} = I_C + I_J + I_R \tag{5}$$

$$= C\frac{dV}{dt} + I_c \sin(\varphi) + \frac{V}{R} \tag{6}$$

$$= C\frac{\hbar}{2e}\frac{\partial^2\varphi}{\partial t^2} + I_c \sin(\varphi) + \frac{1}{R}\frac{\hbar}{2e}\frac{\partial\varphi}{\partial t}. \tag{7}$$

The last step was made using equation (4). I_C is the current through the capacitance C, I_J is the current through the Josephson junction J and I_R is the current through the resistance R. V is the voltage across the parallel combination of ideal junction, capacitance and resistance.

1.3 rf-SQUIDs

A **S**uperconducting **QU**antum **I**nterference **D**evice (SQUID) consisting of a superconducting ring containing a single Josephson junction is called a rf-SQUID (see figure 3).

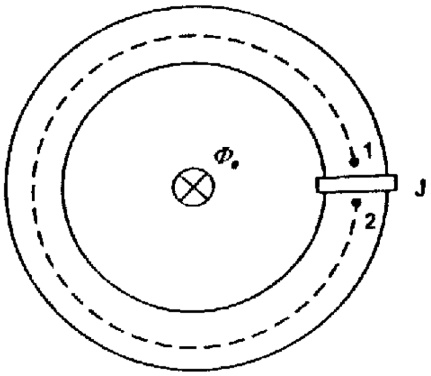

Figure 3: Sketch of a rf-SQUID [1].

In a rf-SQUID the phase difference across the Josephson junction is equal to

$$\varphi = 2\pi \frac{\Phi}{\Phi_0} \tag{8}$$

with the total flux through the ring Φ and the flux quantum Φ_0 [1].
Because of the induced screening current I_{sc} the total flux differs from the externally applied flux Φ_e:

$$\Phi = \Phi_e - LI_{sc}. \tag{9}$$

As the screening current passes through the Josephson junction it behaves according to the Josephson relation in equation (3). Substituting (8) in (3) yields

$$I = I_c \sin\left(2\pi \frac{\Phi}{\Phi_0}\right). \tag{10}$$

Applying this new equation to equation (9) yields

$$\Phi_e = \Phi + LI_c \sin(2\pi \frac{\Phi}{\Phi_0}). \tag{11}$$

This equation gives us the implicit relation between external flux and total flux in the loop shown in figure 4 for $\beta_L > 1$. This parameter is defined as the ratio $\beta_L = \frac{L_{geom}}{L_J}$ with the geometric inductance L_{geom} and the Josephson inductance L_J, which is defined in equation (13). The value β_L of a SQUID strongly influences its behavior.

When, in figure 4, the externally applied flux through the loop is increased starting from $\Phi_e = 0$ there is an induced screening current partially cancelling out the applied flux. In case of a solid ring without a junction the induced current would cancel out the applied flux completely. Due to the presence of the junction the cancellation is only partial because the magnetic field can penetrate into the ring's interior [1]. At a critical value $\Phi_e = \Phi_{ec}$ (point D), however, the system jumps to the next quantum state (point A) because it is now energetically more favorable that one flux quantum enters the loop. At this point A the

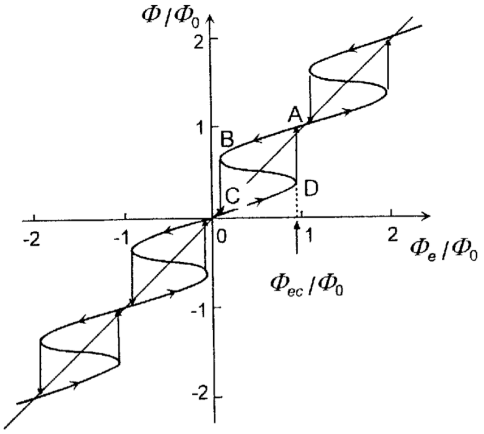

Figure 4: Implicit relation between Φ and Φ_e for $\beta_L > 1$ [1].

total flux Φ through the loop becomes larger than the external flux. To meet equation (11) the screening current has to change its direction.
From point A there are two different ways the system can develop.
If the external flux is increased further the external flux will reach the value $\Phi_e = \Phi_0$. There the total flux is also Φ_0 and according to equation (10) the current is $I = 0$A. Therefore the system is effectively in the same state as in the origin. With further increase of the applied flux the system will go through this process with period Φ_0.
If, however, the external flux is decreased from point A the jumps will start from points analogous to point B. Thus, a cyclic variation of the external flux is accompanied by a hysteresis loop CDABC. The area of the loop is proportional to the energy dissipated in the junction [1].

As we used SQUIDs with $\beta_L < 1$ the hysteretic behavior described above does not occur in our SQUIDs. For different values of β_L the behavior looks as shown in figure 5.

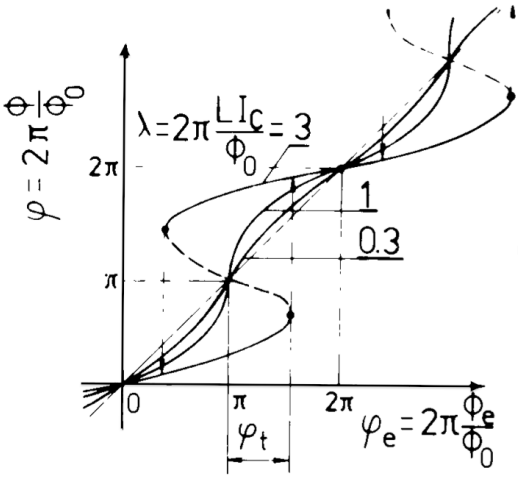

Figure 5: Implicit relation between Φ and Φ_e for different values of β_L (β_L is called λ in this figure from reference [4]).

In the case of a sinusoidally alternating external flux the rf-SQUID can be interpreted as a

regular LC-circuit with the resonance frequency $\omega = \frac{1}{\sqrt{L_{tot}C}}$. In a rf-SQUID L_{tot} is

$$L_{tot} = \frac{L_{geom}L_J}{L_{geom} + L_J} \tag{12}$$

with the geometric inductance of the loop L_{geom} and the Josephson inductance L_J which is

$$L_J = V \cdot \left(\frac{\partial I}{\partial t}\right)^{-1} = \frac{\hbar}{2e} \cdot \frac{1}{I_c \cos(\varphi)}. \tag{13}$$

The last step in equation (13) is derived using the first and second Josephson relation (equations (3) and (4)).
From equation (13) it becomes clear that the resonance frequency of a rf-SQUID is tunable due to the tunability of L_J, i.e. of L_{tot}. From equations (12) and (13) one can see that the total inductance becomes $L_{tot} \approx L_{geom}$ at $\cos(\varphi) \approx 0$. This is the case if $\varphi \approx \frac{\pi}{2}$ or $\varphi \approx \frac{3\pi}{2}$. As the current through the junction is $I = I_c \sin(\varphi)$ it means that $L_{tot} \approx L_{geom}$ holds for currents $|I| \approx I_c$. Why this is relevant will be explained in section 3.

1.4 Metamaterials

Metamaterials are typically constructed of 'atoms' that have an engineered electromagnetic response. The properties of the artificial atoms are often engineered to produce non-trivial values for the effective permittivity and effective permeability of a lattice of identical atoms. Such values include relative permittivities and permeabilities that are less than 1, close to zero, or negative [5].

The first metamaterials were made of an array of split-ring resonators (SRRs). More recent SQUID metamaterials are made of an array of SQUIDs, as shown in figure 8. Both kinds of metamaterials only couple to a magnetic field.

Conventional metamaterials utilize SRRs to influence the dielectric properties by manipulating the effective plasma frequency of the medium.
Substantial ohmic losses in the radio frequency range are one of the key limitations of conventional metamaterials. In contrast to normal metals, superconducting wires and SRRs can be substantially miniaturized while still maintaining their low loss properties [5].

SQUID metamaterials consist of a regular array of SQUIDs. A SQUID can be seen as a quantum analog of the split-ring resonator in which the classical capacitor is replaced by a Josephson junction [5]. This has the main advantage of tunability of the Josephson inductance (see section 1.3).

1.5 Coupling Strength between rf-SQUIDs

The basic notion of the transition from the dynamics of one SQUID to the relative permeability of an array of SQUIDs was shown by Lazarides and Tsironis [6]. It is briefly described in the following.

The normalized flux f trapped inside a SQUID is

$$f = f_{ext} + \beta i \tag{14}$$

with $f = \frac{\Phi}{\Phi_0}$, $f_{ext} = \frac{\Phi_{ext}}{\Phi_0}$, $\beta = \frac{\beta_L}{2\pi} \equiv \frac{LI_c}{\Phi_0}$, $i = \frac{I}{I_c}$. I is the current circulating in the ring and L is the geometric inductance of the ring.
The dynamics of the normalized flux is governed by the equation [6, 7]

$$\frac{d^2 f}{d\tau^2} + \gamma \frac{df}{d\tau} + \beta \sin(2\pi f) + f = f_{ext}. \tag{15}$$

Here is $\gamma = \frac{L\omega_0}{R}$ the dissipation coupled to the SQUID, $\tau = \omega_0 t$ is the time normalized to the resonance frequency $\omega_0 = \frac{1}{\sqrt{LC}}$. R and C are as introduced with the RCSJ model. Furthermore it is $f_{ext} = f_{e0}\cos(\Omega\tau)$ with $f_{e0} = \frac{\Phi_{e0}}{\Phi_0}$ and $\Omega = \frac{\omega}{\omega_0}$.

Lazarides et al. continue by investigating the special case for a frequency close to the resonance frequency, i.e. $\Omega \approx 1$, in the nonhysteretic regime $\beta_L < 1$.
They solve the differential equation for the flux

$$f = f_0 \cos(\Omega\tau + \theta) \tag{16}$$

in the loop with

$$f_0 = \frac{f_{e0} - D}{\sqrt{\gamma^2\Omega^2 + (1-\Omega^2)^2}}, \qquad \theta = \tan^{-1}\left(\frac{-\gamma\Omega}{1-\Omega^2}\right). \tag{17}$$

Here θ is the phase difference between f and f_{ext}.
$D(f_{e0}) = -2\sum_{n=1}^{\infty}[(-1)^n/n\pi]J_n(n\beta_L)J_1(2\pi n f_{e0})$ is a complicated sum, the form of which is not important for our purpose. Lazarides et al. derive it via a Fourier-Bessel series in order to replace the $[\beta\sin(2\pi f)]$ term in equation (15).

Additionally, another special case is investigated, namely the regime with $\gamma \ll 1$ and Ω not very close to the resonance. There holds $\theta \approx 0$.
For $\gamma = 0$, i.e. no dissipation at all, the solution is

$$f = \pm|f_0|\cos(\Omega\tau), \qquad |f_0| = \frac{f_{e0} - D}{|1 - D^2|}. \tag{18}$$

The plus (minus) sign corresponds to a phase shift of 0 (π) of f with respect to f_{ext}. The plus sign is obtained for $\Omega < 1$, the minus sign for $\Omega > 1$. Therefore the flux f is either in phase (+ sign) or in anti-phase (- sign) with f_{ext} depending on Ω [6].
From the regular description of the magnetic field strength B in matter

$$B = \mu_0(H_{ext} + M) \equiv \mu_0\mu_r H_{ext} \tag{19}$$

with the external magnetic field H_{ext}, the permeability constant μ_0 and the relative permeability μ_r. Inserting for the magnetization $M = \frac{AI}{V} = \frac{\pi a^2 I}{d^3}$ with the radius a and the area of each SQUID $A = \pi a^2$ and rearranging for μ_r we get

$$\mu_r = 1 + \frac{\pi a^2}{d^3} \frac{I}{H_{ext}} \tag{20}$$

where d is the periodicity of the SQUIDs in the array and I is the current in the SQUID loop. This is the equivalent description for an array of rf-SQUIDs that form a metamaterial with a specific μ_r.
Using equations (14) and (18) the current I in equation (20) can be replaced. It follows

$$\mu_r = 1 + \pi^2 \frac{\mu_0 a}{L} \left(\frac{a}{d}\right)^3 \left(\pm \frac{|f_0|}{f_{e0}} - 1\right). \tag{21}$$

The prefactor $\widetilde{F} = \pi^2 \frac{\mu_0 a}{L} \left(\frac{a}{d}\right)^3$ depends on the periodicity d between neighboring SQUIDs and can therefore be used as a measure for coupling strength.

2 Measurement setup

2.1 General setup

The setup is shown in figure 6. The setup of our experiment consisted of an Anritsu Vector Network Analyzer (VNA), a chip sample with one dimensional rf-SQUID arrays on it and a superconducting coil providing the constant magnetic field. The sample was fixed at the front end of the short coil with an orientation such that the coil's magnetic field penetrated the SQUIDs' area perpendicularly. The coil current was supplied by an external current source. During the experiments the sample was cooled down to $T = 4.2\text{K} < \text{T}_{\text{c,Nb}}$. The critical temperature of niobium is $T_{c,Nb} = 9.25\text{K}$ [1].

2.2 Measurement procedure

During our experiments the VNA sent a microwave signal from point 1 (output) through the sample to point 2 (input). On the way there, the signal passed a cold -30dB attenuator to reduce its power at the sample. This was necessary because the VNA could not supply the low power we needed. The signal was coupled to the coplanar transmission line on the chip. The magnetic component of the field around the coplanar transmission line coupled inductively to the SQUIDs.
Because of this coupling a current was induced in the SQUIDs. The SQUIDs in turn coupled with each other magnetoinductively. Because it requires energy to drive the induced current oscillations the amplitude of the microwaves in the central line decreases significantly at resonance. The exact conditions for the energy dissipation are described in chapter 3.5.
The VNA uses an oscillator to produce a frequency sweep over time which was supplied to our sample. The electronically controlled frequency sweep allowed automatic measurements over a preset frequency range. The signal transmitted through the sample was measured by the VNA. A Python script running on the PC was used as control unit for setting the parameters at the VNA. The microwave power and frequency were varied.
Furthermore the external magnetic flux was varied in discrete steps between each frequency sweep by changing the current I_b through the coil.
Before the microwave signal arrived at the VNA point 2 it was damped again by a cold -10dB attenuator to reduce reflections and afterwards amplified by a $+30$dB amplifier at room temperature.

Due to the oscillatory nature of the magnetic field of the microwave signal the average external magnetic field at the sample was given only by the magnetic field due to the coil.

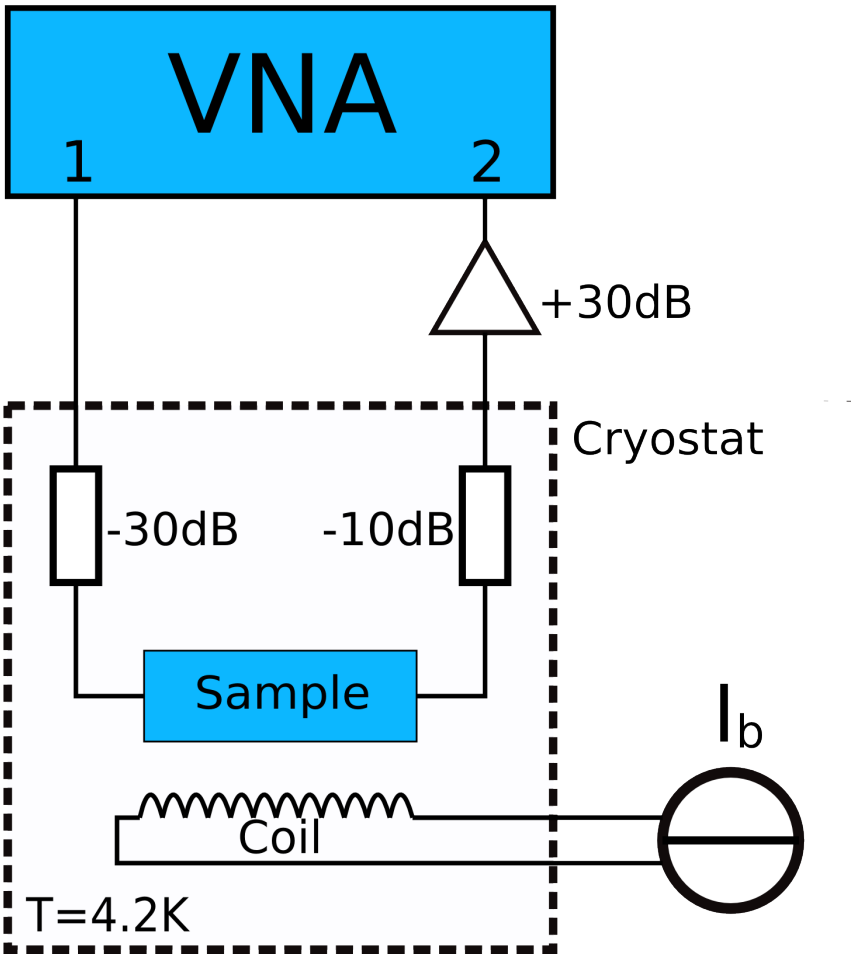

Figure 6: Sketch of the setup.

2.3 Coplanar transmission line

A sketch of our symmetric **C**o**P**lanar **T**ransmission **L**ine (CPTL) together with the rf-SQUIDs is depicted in figure 7.
A CPTL is characterized by conductor planes, which are placed on top of the substrate. The symmetric CPTL consists of a central line and two ground planes [8]. Our central line has a width of $w = 112\mu$m and a thickness of $h = 300$nm. There is a 82μm wide gap, from the edge of the central line to each of the ground planes, for the SQUID arrays to be placed in. All conductor planes consist of a niobium layer on top of a Si-substrate with permittivity $\epsilon_r = 11.9$ [8].
For a CPTL the effective permittivity [8] has to be applied, which is defined as $\epsilon_{r,eff} = \frac{\epsilon_r+1}{2}$. The electric field lines of a CPTL are between the central line and the ground planes. The magnetic field lines surround the central line and go through the substrate in the gap between the central line and the ground planes [8].

We assume that all the SQUIDs in the array are exposed to a similar magnetic field caused by the CPTL. This is satisfied if the wavelength λ of the microwaves on the CPTL is greater than the length of the array l_{array}. To be specific the condition $\frac{\lambda}{2} \gg l_{array}$ has to be met.
To evaluate this we estimate the wavelength using the approximation

$$\lambda = \frac{c}{n_{eff} \cdot f} = 6.9\text{mm} \tag{22}$$

with an effective refractive index $n_{eff} = \sqrt{\epsilon_{r,eff}}$, the speed of light c and the operating frequency f. The chip with the arrays on it has a length of $l_{chip} = 5$mm. However, the SQUIDs do not fill the entire length of the chip.
The arrays with periodicities of 55μm and 90μm only have lengths of $l_{array,55} = 0.82$mm and $l_{array,90} = 1.3$mm. Thus the above condition is met.
The array with the largest periodicity (225μm) has a length of about $l_{array,225} = 3.2$mm. This array is much longer than the other two arrays. Thus for this array holds $l_{array} \approx \frac{\lambda}{2}$ and the above condition is not met. This means that the SQUIDs in this array are not all exposed to a similar magnetic field and are not driven by a similar force.

2.4 Sample layout

Each chip we used had three transmission lines on it (see figure 8). In the two gaps above and below along each transmission line, a one-dimensional array of rf-SQUIDs was placed. Figure 7 shows a sketch of such a transmission line. In the middle there was the central line, above and below it was one SQUID array in each case. Respectively further outward was the ground plane. The chip substrate was made of Si. The SQUIDs and the transmission line were made of niobium. The Josephson junction in the SQUIDs was made of Nb-Al_2O_3-Nb tri-layers. The dimensions of the central line were: width $w = 112\mu$m, height $h = 300$nm and length $l = 5$mm. The gap between the central line and the ground plane was $g = 82\mu$m wide.
A sketch of the SQUIDs used in our experiments is shown in figure 9. Our SQUIDs had a hysteresis parameter of $\beta_L = 0.9 < 1$ [3].
As area of the SQUID loop an effective area has to be used: $A = A_{eff} = 35\mu\text{m} \cdot 37\mu\text{m}$. This effective area is larger than the free space inside the loop because flux focussing has to be taken into account because in superconductors the magnetic field is pushed out of the material. Therefore the flux through the hole is greater than the magnetic field times the area of the hole. As an estimate we assumed that the effective area includes the free space inside the loop and half of the area of the SQUID material because half of the flux through the SQUID material will be pushed inside the loop and half of the flux will be pushed outside the loop.

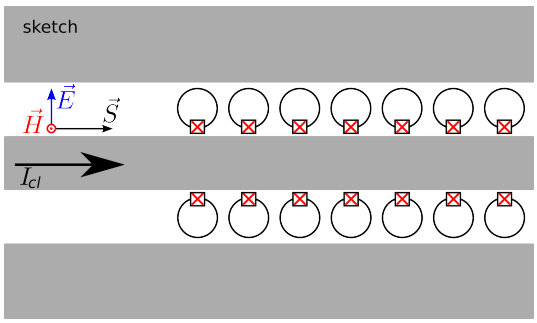

Figure 7: Design sketch of the sample [9].

The preparation of the samples was a process requiring several steps. First, the chip had to be glued to a copper **P**ortable **C**ircuit **B**oard (PCB). After the glue had dried, each transmission line on the chip was bonded with thin wires to the corresponding area on the PCB. The gold pads, on the left and right side of each transmission line, were used for bonding (see figure 8).
As each transmission line had a separate connection to the PCB it allowed us to investigate each transmission line separately.

An original design sketch of a chip is shown in figure 8. The periodicity of the SQUIDs is different for each of the three transmission lines. We used two different chip designs and gathered data from three different transmission lines with periodicities of 55μm, 90μm and 225μm.
At the bottom of each chip there were dc test structures which are magnified in figure 10. The test structures incorporated a single dc-SQUID on the right as well as a single junction on the left. We used them to check the quality of the chip and to find fabrication defects. We did this by measuring the current-voltage characteristics (I-V curve) of the junction

and calculating the critical current I_c to make sure that it met the specified value. This procedure is explained in section 3.1.

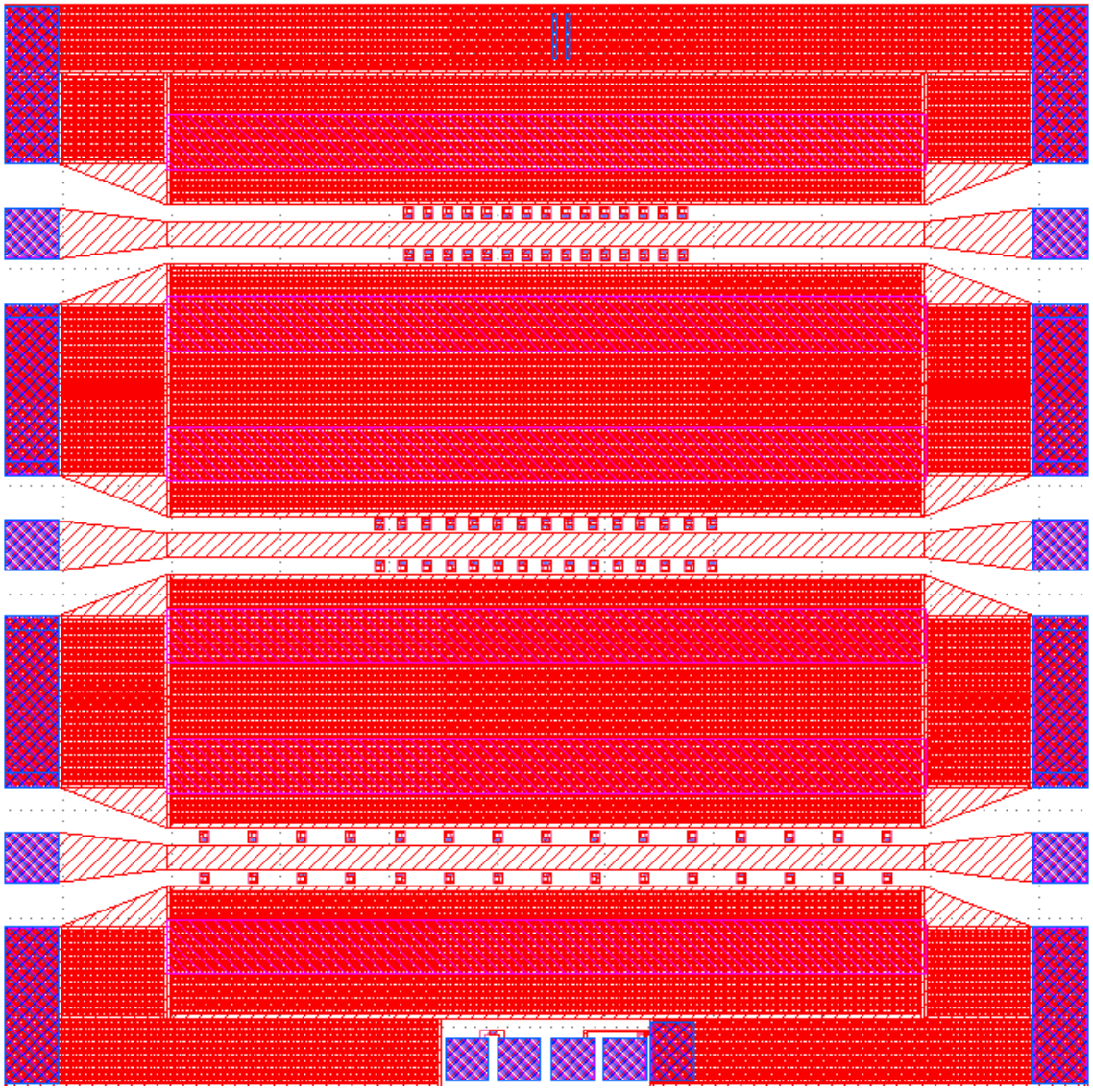

Figure 8: Chip with SQUID arrays on it [9].

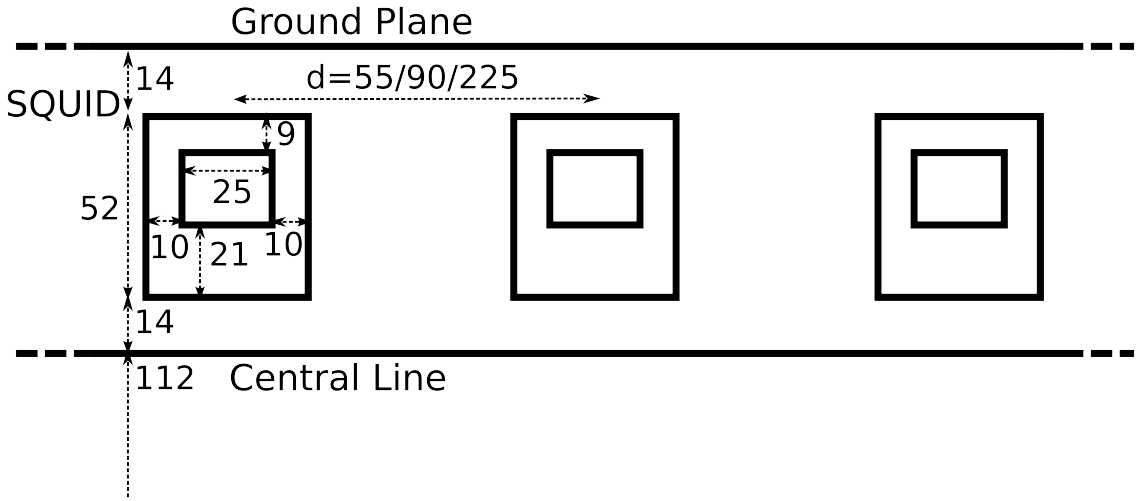

Figure 9: SQUID array sketch with dimensions in μm.

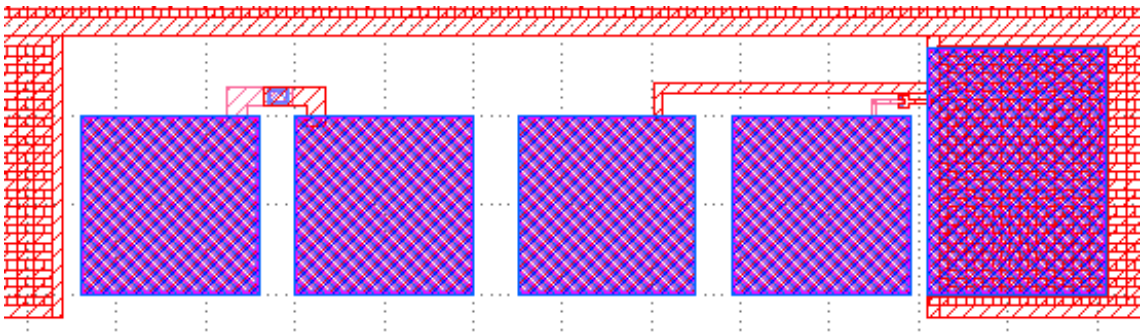

Figure 10: DC test structures with bonding pads - on the left: a single junction; on the right: a DC-SQUID [9].

3 Results

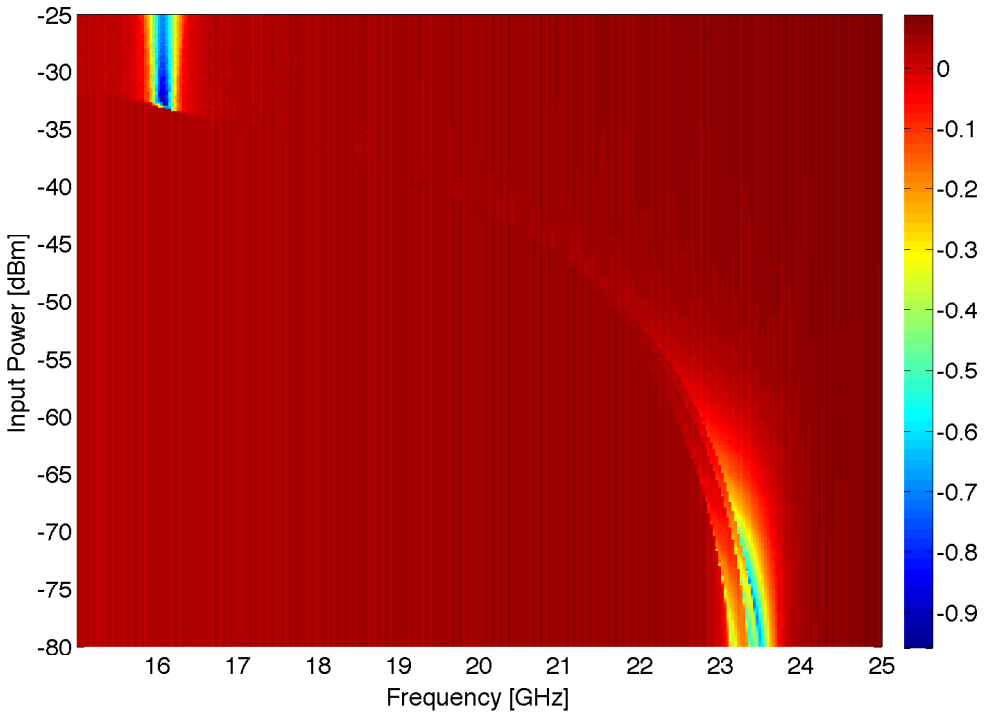

Figure 11: Simulation of transmission [dB] over a wide input power and frequency range [10].

The phenomenon we investigated was first assumed in a simulation [10] like the one in figure 11.

It illustrates the behavior of a SQUID transmission line with four rf-SQUIDs over a wide power and frequency range. As input for the simulation the original design parameters of our SQUIDs were used. The SQUIDs had a periodicity of 90μm. The figure shows the transmission in color code depending on the applied power and frequency. The color bar marks the transmission in units of [dB].

There are two different behaviors in the picture with a gradual transition in between. At low power values there are several narrow bands. There are different bands because the SQUIDs have slightly different resonance frequencies, which is the case on our chip due to fabrication tolerances, as is explained below. This effect was also taken into account in the simulation.

The bands all move to lower frequencies at higher power values and furthermore move closer together at higher power values. At a certain point on the frequency axis all bands unite and form a deep dip. This point corresponds to the input frequency $\omega = \frac{1}{\sqrt{LC}}$, with $L = L_{geom} = 58\text{pH}$ and $C = 1.8\text{pF}$ being the inductance and capacitance of the SQUID loops without the Josephson junction, that is of a simple closed metal ring. This dip is tapered along the frequency axis towards lower power values and expands towards higher power values.

All the SQUIDs have very similar L_{geom} and C and therefore a very similar resonance frequency at high power values. As the area of the Josephson junction, however, is subject to greater fabrication differences the critical current, the capacity and the inductivity of the

junctions varies between the SQUIDs. Because of this the SQUIDs have different resonance frequencies at low power values.

Running several simulations at various external flux bias values one can see that the power at which the small bands unite and the big dip begins, depends on the externally applied flux. That is, it moves up and down with period Φ_0. The goal of our experiments was to investigate the influence of the periodicity of the SQUIDs on the power interval in which flux dependence occurs, i.e. in which the big dip moves up and down when changing the applied external flux.
The actual analysis of our experiment however will be carried out in a power versus flux bias diagram.

The simulation in figure 11 is very instructive as it shows the general resonance behavior of the SQUIDs over a much wider power range than we could measure in our experiment.
A corresponding diagram of our experimental data is shown in figure 12. It illustrates the data of a SQUID array with periodicity $d = 225\mu$m at the external flux $\Phi_e = 0 \cdot \Phi_0$. The numbers at the color bar indicate much lower transmission than in the simulation. This is due to the fact that there are only four SQUIDs placed in each transmission line in the simulation, whereas there are fifteen in each transmission line in the real measurement. Furthermore attenuators were used in the real measurement that are not part of the simulation. As this also lowers the transmission the standardization differs between the two figures.
What can also be seen is that the dip goes to much lower power values in the real measurement. This is probably due to an offset in external flux, due to which $I_b = 0$A does not represent $\Phi_e = 0 \cdot \Phi_0$ in our measurement. However, as we cannot specify the offset in the flux bias, we will use $\Phi_e = 0 \cdot \Phi_0$ as if it corresponded to $I_b = 0$A in the following.
In figure 13 the same measurement is shown as above but at the external flux $\Phi_e = \frac{\Phi_0}{4}$. It can be seen that the dip is moved up towards higher power values here.
As our experiments were carried out at relatively high power values the average currents at which we operated were $I \approx I_c$. Therefore $L_{tot} \approx L_{geom}$ holds in all our considerations. This means that we can only observe the big dip in our measurements. Its form and position in figures 12 and 13 is as expected in the considerations above. The reason we measured at such high power values was that the VNA could not operate at lower power values. To reduce the power at the sample external attenuators were added to the setup. With too much attenuation, however, the signal to noise ratio would have become too bad.

The power range used in the measurements was such that the interval in which the flux dependence of the transmission occurred could be observed. This means a power range at the VNA from -35dBm to about 0dBm which translates to power values at the sample between -65dBm and -30dBm.
The frequency was varied in a narrow range of up to 300MHz around the resonance frequency of about $f_{res} = 17$GHz (for f_{res} see figures 18 and 19) of the SQUIDs.

The bias current I_b of the coil was chosen between -3μA and 2μA. The range of the corresponding magnetic field caused a variation of the flux through the SQUID loop of about two flux quanta.

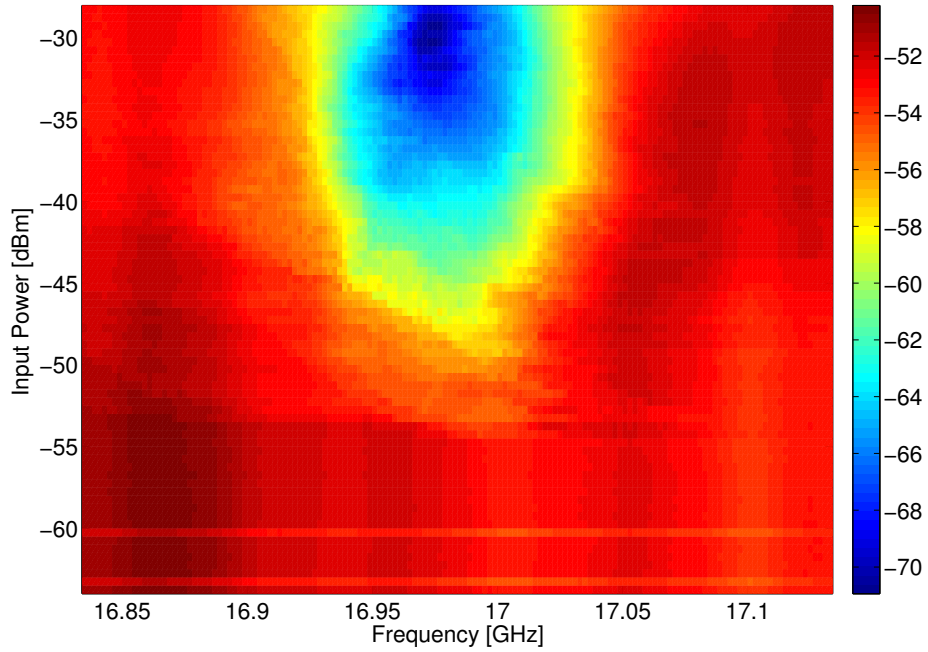

Figure 12: Input Power at the Sample vs. Frequency for SQUID periodicity $d = 225\mu$m at the external flux $\Phi_e = 0 \cdot \Phi_0$ (calculated from the bias current through the coil).

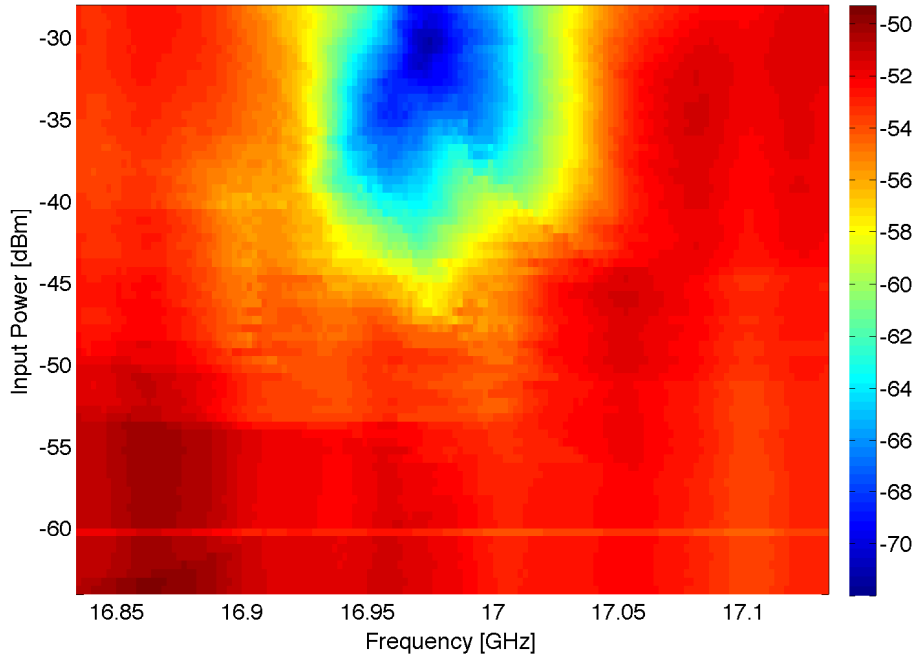

Figure 13: Input Power at the Sample vs. Frequency for SQUID periodicity $d = 225\mu$m at the external flux $\Phi_e = \frac{\Phi_0}{4}$ (calculated from the bias current through the coil).

3.1 Critical current I_c of a Josephson junction

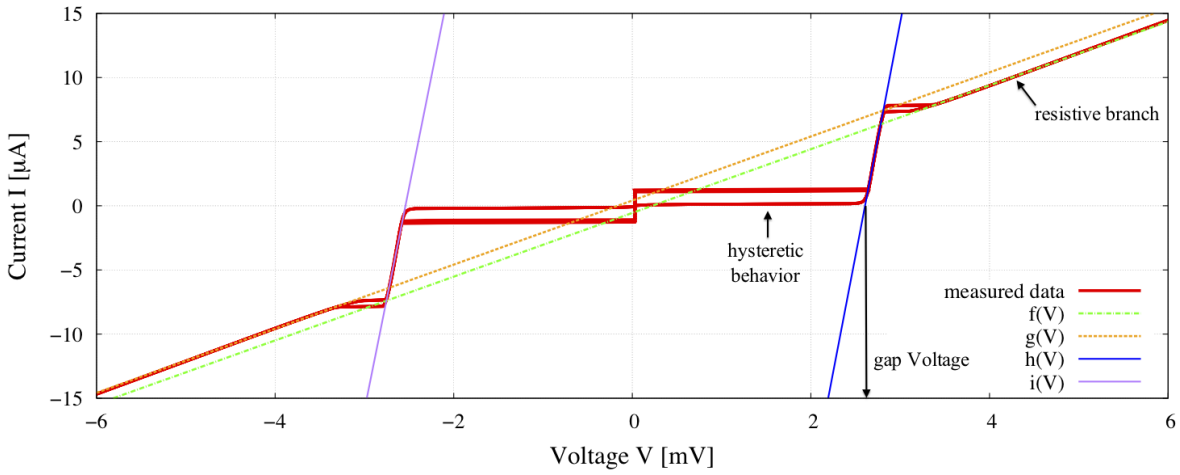

Figure 14: I-V measurement of a Josephson junction. With fits $f(V) = 2.5V - 0.6$, $g(V) = 2.5V + 0.4$, $h(V) = 36.3V - 94.6$, $i(V) = 34.7V + 88.1$.

For measuring the I-V curve of a Josephson junction within our test structures we sent a current through a junction and measured the voltage as a function of the current. This was done using a 4-point measurement. The measured data can be seen in figure 14 together with the fits made for the following calculations. The hysteretic behavior, the gap voltage V_{gap} and the resistive branch are indicated.

Starting at V_{gap} Ohm's law $I = \frac{V}{R}$ applies as can be seen in the I-V curve in figure 14.
V_{gap} is the voltage at which the junction behavior passes into the normal resistive state. R is the inverse of the slope of the I-V curve above V_{gap}. With Gnuplot linear fits to the measured data in the appropriate intervals were made. We get $V_{gap} = 2.6$mV by calculating the null of $h(V)$ and $i(V)$ and taking the mean value. $R = 401.4\Omega$ is the inverse of the mean value of the slope of $f(V)$ and $g(V)$.
Using the Ambegaokar-Baratoff formula [11]

$$I_c = \frac{\pi}{4} \cdot \frac{V_{gap}}{R} = 5.0 \cdot 10^{-6} A \tag{23}$$

we get $I_c = 5.0 \cdot 10^{-6} A$. The junctions were actually designed for $I_c = 8.0 \cdot 10^{-6} A$. This discrepancy is due to fabrication tolerances but was consistently observed for all measured junctions.

The Stewart-McCumber parameter β_c [3] of the measured junction as for all our junctions is

$$\beta_c = 2\pi \frac{I_c R^2 C}{\Phi_0} = 4.4 \cdot 10^3. \tag{24}$$

with $C = 1.8$pF. Because of $\beta_c \gg 1$ the I-V curve has a hysteretic behavior [3].

3.2 Mutual inductance M_{21} and coupling coefficient $\widetilde{F}$

3.2.1 Mutual inductance calculated with FastHenry

To compare the coupling coefficient (as introduced in chapter 1.5) to another measure of SQUID interaction namely the mutual inductance between two SQUIDs, the inductance extraction software FastHenry was used. The mutual inductance is defined in equation (26). FastHenry was supplied with the physical dimensions of the array as shown in figure 9. The program calculated via a finite element method the mutual inductances between the SQUIDs for the specified dimensions and the different periodicities.
The resulting mutual inductances M are displayed in table 1. The mutual inductance, by definition, has a negative value whereas the coupling coefficient has a positive value. It is useful to compare the absolute values. The absolute values of the mutual inductances calculated with FastHenry are plotted in figure 15 versus the distance d of the SQUIDs, i.e. their periodicity. The red plus signs in this figure show the mutual inductance between two nearest neighbors and the blue crosses show the mutual inductance between two next but one nearest neighbors. M_1 is the fitted curve for the mutual inductance between nearest neighbors (solid red line), M_2 is the fitted curve for the mutual inductance between next but one neighbors (solid blue line). The data points were calculated by FastHenry, the fits were calculated using Gnuplot.

This figure shows that the dependence of the absolute value of the mutual inductance M on the distance d between the SQUIDs is well described by a polynom of the form $M = c \cdot d^{-3}$ with some positive constant c. As the mutual inductance becomes smaller at greater distances the current induced by one SQUID in another SQUID also becomes smaller at greater distances.

Because of the $M \propto d^{-3}$ dependence the absolute values of the mutual inductance for the two different cases differ the most at low periodicities. In relative values the mutual inductance between two next but one neighbors is always just $\frac{M_2}{M_1} = \frac{2.4 \cdot 10^{-8}}{2.6 \cdot 10^{-7}} \approx 9.2\%$ of the mutual inductance between two nearest neighbors. Therefore the coupling effect of the next but one neighbor is negligibly small in comparison with the nearest neighbor.

Table 1: Mutual Inductance depending on the SQUIDs distance (calculated with FastHenry)

	Mutual Inductance M_{21} in 10^{-13}H	
d [μm]	nearest neighbor	next but one neighbor
55	-16.53	-1.479
70	-6.70	-0.689
90	-2.84	-0.314
110	-1.48	-0.169
120	-1.12	-0.129
140	-0.69	-0.080
160	-0.45	-0.052
175	-0.34	-0.040
190	-0.27	-0.030
210	-0.19	-0.022
225	-0.16	-0.018

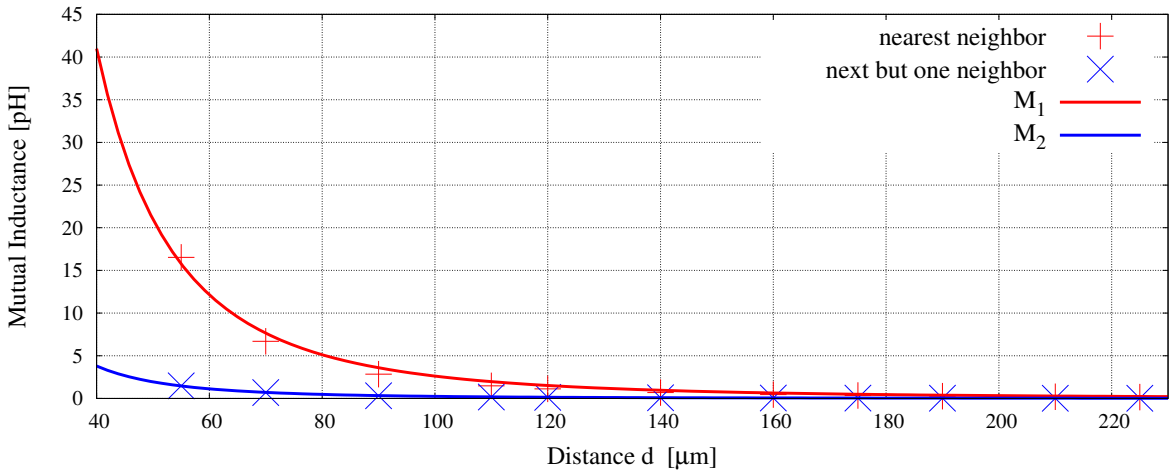

Figure 15: Mutual Inductance depending on the SQUIDs distance. With fits $M_1(d) = 2.6 \cdot 10^{-7}\mathrm{Hm}^3 \cdot \mathrm{d}^{-3}$ and $M_2(d) = 2.4 \cdot 10^{-8}\mathrm{Hm}^3 \cdot \mathrm{d}^{-3}$, both with d in [m].

3.2.2 Calculation of the coupling coefficient $\widetilde{F}$

The derivation of the dependence of the coupling constant $\widetilde{F}$ on the period d of the SQUIDs was already shown in chapter 1.5. The resulting dependence was

$$\widetilde{F} = \pi^2 \left(\mu_0 \frac{a}{L}\right) \left(\frac{a}{d}\right)^3 \propto d^{-3}. \tag{25}$$

$\widetilde{F}$ is calculated for a ring shaped SQUID. The radius $a = 20.3\mu$m is chosen such that the area of the ring shaped SQUID matches the actual area of our SQUIDs. Furthermore the geometric inductance of our SQUIDs is $L = 5.9 \cdot 10^{-11}$H

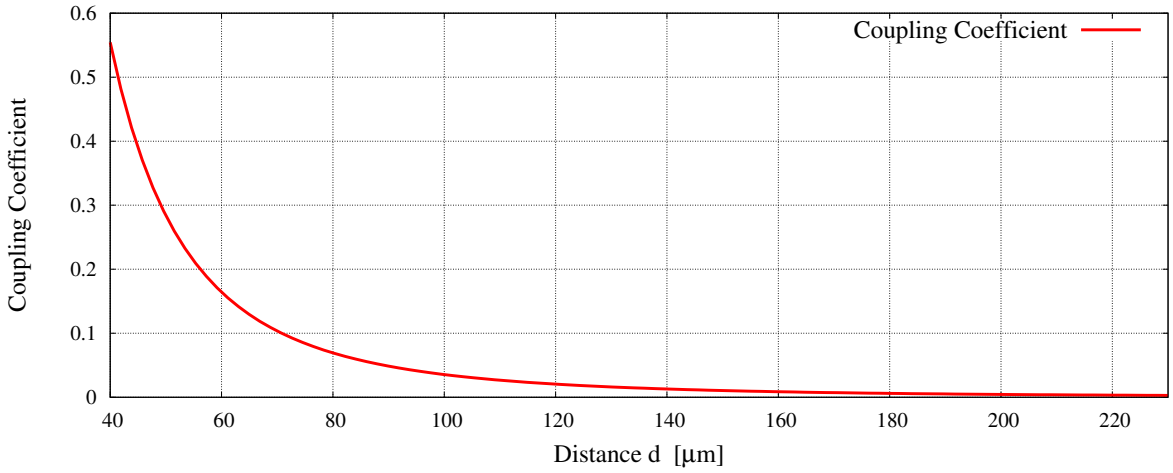

Figure 16: Coupling coefficient $\widetilde{F}$ depending on the SQUIDs distance according to equation (25). $\widetilde{F} = 3.5 \cdot 10^{-14}\mathrm{m}^3 \cdot \mathrm{d}^{-3}$ with d in [m].

3.2.3 Comparison of the results

The mutual inductance as well as the coupling coefficient are both measures for the coupling strength.

As both figures (15) and (16) show the same dependence on the distance ($\propto d^{-3}$) the conclusion can be drawn that there is a connection between the coupling coefficient and the mutual inductance. Their information is analogous. In fact the difference is just a constant factor. Therefore it holds $\widetilde{F} = z \cdot M_{21}$ with $z = 1.4 \cdot 10^{-7} \frac{1}{\mathrm{H}}$ for nearest neighbors.
The coupling coefficient on the one hand is derived from theoretical calculations using reference [6], the mutual inductance on the other hand can be measured experimentally or via a simulation, as we did.

3.3 Induced current in a SQUID

3.3.1 Current induced by another SQUID

The definition of the mutual inductance M_{21} is

$$M_{21} = \frac{\Phi_{e2}}{I_1} \tag{26}$$

where $I_1 \in [0,I_c]$ is the current in a SQUID 1 in figure 9 and Φ_{e2} is the resulting external flux through the neighboring SQUID 2. Rearranging the equation it follows

$$\Phi_{e2} = M_{21} \cdot I_1. \tag{27}$$

In order to calculate the maximum SQUID-on-SQUID influence we will take the maximum value for the current $I_1 = I_c$. As already described, the mutual inductance M_{21} of two nearest neighbor SQUIDs was calculated with FastHenry.
With the well known relation derived in chapter 1.3

$$\Phi_{e2} = \Phi_2 + L \cdot I_c \cdot \sin\left(2\pi \frac{\Phi_2}{\Phi_0}\right) \tag{28}$$

with the geometric inductance L and the critical current I_c we can determine the effective flux Φ_2 through the second SQUID. For doing this one can make the approximation $\sin(a{\cdot}x) \approx a{\cdot}x$ because $\Phi_2 \ll \Phi_0$ holds. Solving equation (28) after the approximation yields

$$\Phi_2 = \frac{\Phi_{e2}}{1 + LI_c \frac{2\pi}{\Phi_0}}. \tag{29}$$

With the values for Φ_{e2} from equation (27) using the respective values of M_{21} for the different SQUID periodicities we get the values for Φ_2 and thus we get the induced currents via

$$I_2 = I_c \sin\left(2\pi \frac{\Phi_2}{\Phi_0}\right) \tag{30}$$

as shown in table 2 which shows the induced currents I_2 and the mutual inductances M_{21} used for calculating Φ_{e2} for each periodicity. For the calculation were also used $L = 5.9 \cdot 10^{-11}$H and $I_c = 5\mu$A.

Table 2: Mutual Inductances M_{21} and induced currents I_2 calculated for three periodicities d using equation (30)

d [μm]	55	90	225
M_{21} [H]	$1.7 \cdot 10^{-12}$	$2.8 \cdot 10^{-13}$	$1.6 \cdot 10^{-14}$
I_2 [A]	$6.6 \cdot 10^{-8}$	$1.1 \cdot 10^{-8}$	$6.3 \cdot 10^{-10}$
I_2/I_c	$1.3 \cdot 10^{-2}$	$2.3 \cdot 10^{-3}$	$1.3 \cdot 10^{-4}$

3.3.2 Current induced by the central line

Now, how many flux quanta are induced in any given SQUID by a current flowing through the central line?
We can calculate this analogously to chapter 3.3.1. For this we need the mutual inductance $M_{cl,s} = 5.2 \cdot 10^{-12}\text{H}$ between the central line and a SQUID. This mutual inductance was calculated with FastHenry. Furthermore we need the current I_{cl} through the central line which is approximately calculated from $P = U \cdot I = Z \cdot I^2$ with a typical input power $P = -50\text{dBm} = 10^{-8}\text{W}$ and the impedance $Z = 50\Omega$ of the central line.

$$I_{cl} = \sqrt{\frac{P}{Z}} = \sqrt{\frac{10^{-8}\text{W}}{50\Omega}} = 1.4 \cdot 10^{-5}\text{A}. \tag{31}$$

With this we can calculate the external flux Φ_{es} from the central line through the SQUID

$$\Phi_{es} = M_{cl,s} \cdot I_{cl}. \tag{32}$$

Proceeding with Φ_{es} analogously to chapter 3.3.1 yields the induced current $I_{SQUID} = 4.6 \cdot 10^{-6}\text{A} = 0.93 \cdot \text{I}_\text{c}$.

3.3.3 Comparison of the results

The induced current by another SQUID for the smallest distance 55μm in table 2 is about seventy times smaller than the induced current by the central line at the input power $P = -50$dBm. This suggests that the effect of coupling SQUIDs is small even for the closest distance. For the greater distances 90μm and 225μm the induced current is only one thousand times and ten thousand times smaller than the induced current by the central line.

3.4 Flux through a SQUID loop caused by I_b

Now, we calculate what bias current I_b in the coil is needed to cause a magnetic field B that creates a flux $\Phi = \Phi_0$ in the SQUID loop. The calculation is rather straightforward:

$$\Phi = \vec{B} \cdot \vec{A} = BA \tag{33}$$

with the effective area of the loop $A = 1.3 \cdot 10^{-9} \mu\text{m}^2$ and the magnetic field $\vec{B}$. The sample is positioned at one end of a short coil in such a way that the magnetic field of the coil penetrates it perpendicularly. The superconducting coil's resistivity is $R = 0\Omega$. Its length is $L = 0.01\text{m}$ and $N = 1000$.
The corresponding magnetic field is [12]

$$B(z = \pm L/2) = \frac{\mu_0 \cdot N \cdot I_b}{2L} \cdot \frac{L}{\sqrt{R^2 + L^2}}. \tag{34}$$

Solving equation (34) for I_b and substituting $\Phi = \Phi_0$ and B from equation (33) we get

$$I_b = \frac{2L}{\mu_0 \cdot N} \cdot \frac{\sqrt{R^2 + L^2}}{L} \cdot \frac{\Phi_0}{A} = 2.5 \cdot 10^{-5}\text{A}. \tag{35}$$

Therefore the current $I_b = 2.5 \cdot 10^{-5}\text{A}$ is expected to cause one flux quantum Φ_0 to thread the area of a SQUID. We will see in chapter 3.6 that this is roughly the value we found experimentally.

3.5 Influences on transmission

When a harmonic oscillator is driven by an external force, the amplitude of the oscillations depends on the amplitude and the frequency of the driving force.
In the same way the currents in the SQUIDs can be seen as LC oscillators that are being "driven", i.e. induced, by the external flux threading them. This external flux stems from a magnetic field around the central line that penetrates the SQUIDs perpendicularly. Thus the microwaves supply the energy for driving the oscillations. Because of this the microwaves significantly lose energy at resonance. Therefore there is a dip in transmission.
As the amplitude of the induced current is maximal close to the resonance frequency of the SQUIDs the power transmission through the transmission line is minimal there. Furthermore the transmission will be smaller for higher power values through the central line as this power is to be seen as the driving force for the magnetic field through the SQUIDs.
Considering the specific behavior of currents in SQUIDs we have to take into account that the current that can be induced in a SQUID in the superconducting state is dependent on the flux threading it, as seen in equation (10).

Evidence for the above expectations is given in the following.
Figures 18 and 19 show the transmission through the transmission line for SQUIDs with a periodicity of 225μm. The flux through the loop is the same in both diagrams. The bias current through the coil is $I_b = -1.8\mu$A. The dip in transmission is deepest for frequencies close to the resonance frequency of about 17GHz. In addition, the dip in transmission is deeper at higher input power (e.g. -29dBm in figure 19) than at lower input power (e.g. -39dBm in figure 18). Far away from the resonance frequency there is no significant difference between different power values.
The difference between the highest and the lowest transmission value over the measured frequency interval will be called the "depth of the dip in transmission" in the following.
The errors of our measurements can be analyzed best in figures 18 and 19. The curves are very smooth and do not show large irregularities. The smoothness of the curves indicates a low noise level and shows that it is possible to analyze the measured data qualitatively.

In figure 17 the transmission is shown color coded in dependence of the frequency of the microwave signal as well as in dependence of the external magnetic flux bias, i.e. the coil current I_b. The periodic behavior of the transmission in flux is clearly visible. We expected these results from our considerations above. They hold true for all used SQUID periodicities.

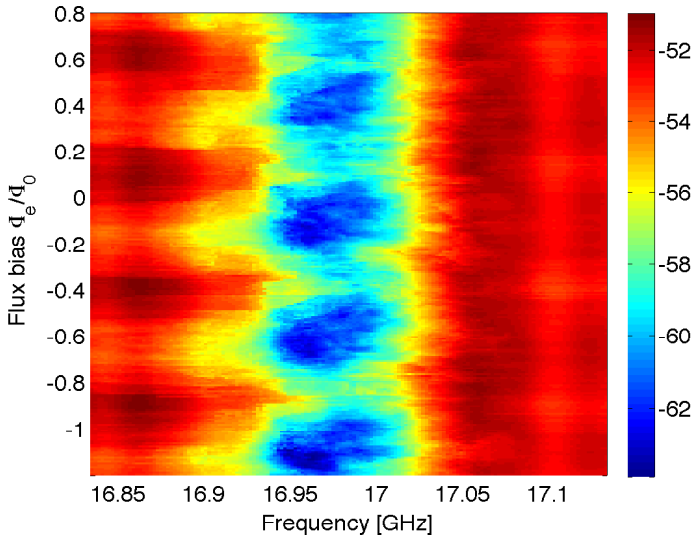

Figure 17: Color coded transmission S_{21} [dBm] for a SQUID periodicity of 225μm at the input power $P = -33.5$dBm at the sample.

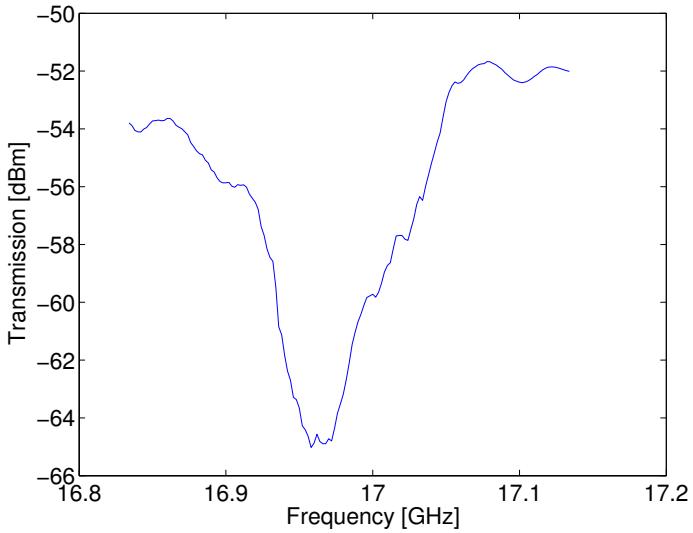

Figure 18: Transmitted power for a SQUID periodicity of 225μm at the input power $P = -39$dBm at the sample.

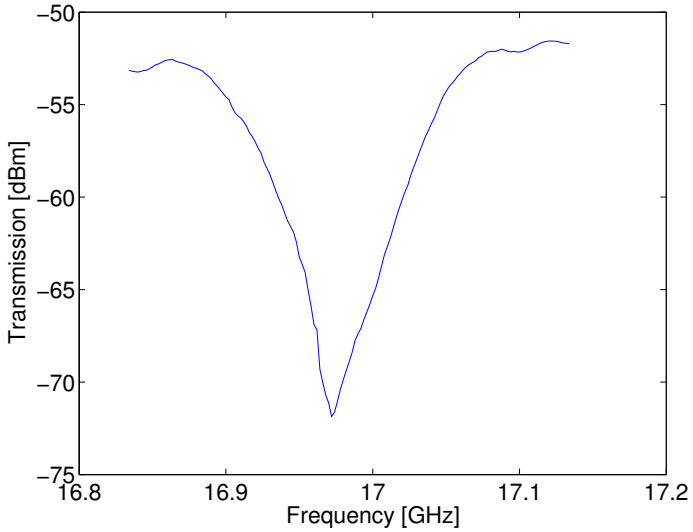

Figure 19: Transmitted power for a SQUID periodicity of 225μm at the input power $P = -29$dBm at the sample.

3.6 Transmission results for different periodicities

Figures 20, 21 and 22 show the experimental results for the periodicities $d = 55\mu$m, $d = 90\mu$m, $d = 225\mu$m. At each point of the power versus flux bias plane the minimal and maximal transmission was determined over the measured frequency interval. The difference between this minimal and maximal transmission, i.e. the depth of the dip in transmission, was then calculated and is shown color coded.

The power vs. flux bias diagrams have a flux axis (in units of Φ_0) which was calculated from the actually set values for the current I_b. The flux axis was rescaled using the conversion factor

$$\Phi_e = \frac{I_b}{2.5 \cdot 10^{-5}\text{A}} \cdot \Phi_0 \tag{36}$$

with the actually set value for the current I_b. The value $2.5 \cdot 10^{-5}$A is derived in section 3.6.1. The same conversion factor is used for all three diagrams because the same periodic behavior of the transmission in flux is expected and confirmed by the figures.
Equation (36) yields $\Phi_e = 0 \cdot \Phi_0$ for $I_b = 0$A. As can be seen in the figures, however, there is an offset in the external flux.

In the three diagrams there are dark horizontal lines drawn. Between these lines, i.e. between the two power values at which the lines are drawn, the depth of the dip in transmission varied more, depending on flux bias, than the specified limit value. This limit value means that the deepest dip at a certain power has to be 5.25dB deeper than the flattest dip at the same power. In this case the transmission at the corresponding input power is considered flux dependent. The chosen limit value in all three figures is 5.25dB.

Following a line along a constant power over all flux bias values, the power values at which the colors do not change much, have only a little change in the difference between maximal and minimal transmission. This means that the depth of the dip in transmission is constant. Therefore the induced oscillating currents are neither much excited nor much inhibited by the externally applied flux from the coil. It is noticeable that the depth of the dip in transmission depends on the external flux only in a certain range of power values. For power values very high or very low there is no dependence on the external flux. Let us analyze three different power ranges on the basis of figure 23. The blue and yellow area in this figure show the dip in transmission, as was explained for figures 12 and 13. With changing flux bias values the dip in this illustration moves up and down, along the input power axis, with period Φ_0. If the dip moves up it means that the blue and yellow area do not reach as far down to low power values as before. Therefore there is a higher transmission now, in the newly red area, than before. Thus the depth of the dip in transmission has changed in just that area in which the colors have changed. If the dip in the figure moves down the same thing happens vice versa.
However, this dip only moves within a certain power range. Therefore if one measures at a power corresponding to line number 1 in figure 23 there is no flux dependence measurable. This is the case because the dip does not move that far up and the transmission is thus relatively constant for such high power values. The same thing happens for power values corresponding to line number 3. The dip never moves that far down. If one measures at power values corresponding to line number 2, which lies within the power range in which the dip moves, there is a flux dependence detectable because transmission changes with the externally applied flux.

It is interesting, that if one lowers the input power even further, far below the power values at which we measured, there comes a point at which a flux dependence of transmission is to be seen again. This can be seen in the simulation in figure 11. At the lowest power values there are several bands corresponding to the different resonance frequencies of the single SQUIDs. As we have seen in section 1.3 the resonance frequency of a SQUID is tunable due to the flux dependence of the Josephson inductance. Thus, if one changes the flux, the resonance frequencies will be different and therefore the narrow bands will shift towards different frequencies.
When looking at the simulation, one can see that the narrow bands go from the lowest power all the way up to the power at which the big dip begins. This means that there is a flux dependency to be expected in all of that range. Because the dip is not very deep in the intermediate power region, however, we could not measure the flux dependency there.

There are some irregularities in figures 20, 21 and 22.
As the flux bias was varied in wider steps in the measurement for $d = 55\mu$m, figure 20 shows a relatively low resolution compared to the respective figures of the other periodicities. Despite this one notices some very regularly appearing horizontal stripes. They do not seem to have a physical meaning but seem to stem from errors in the measurement, which are not known.
In figures 20 and 21 the red areas of high transmission are relatively clearly circumscribed compared to figure 22 in which there is relatively little change in transmission for different flux bias values below power values of about -50dBm at the sample. This is probably an effect of noise.

The bandwidth set at the VNA was 30kHz for all three measurements. The step size in I_b was 10μA for all three measurements.

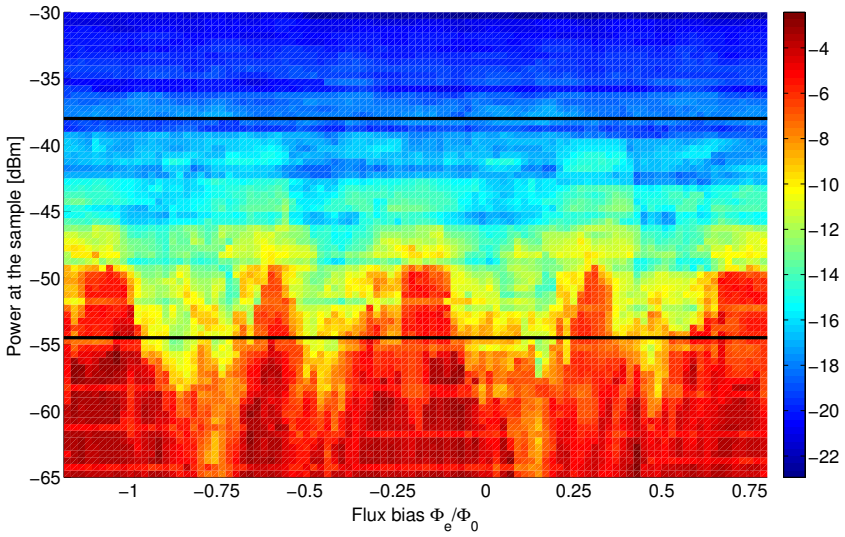

Figure 20: Input power at the sample vs. flux bias for a SQUID periodicity of 55μm. The color code indicates the depth of the dip [dB] (over the measured frequency interval) for each point in the power vs. flux bias plane (see text). The black horizontal lines enclose the power range, within which the change in depth of the dip in transmission over all flux bias values exceeds 5.25dB.

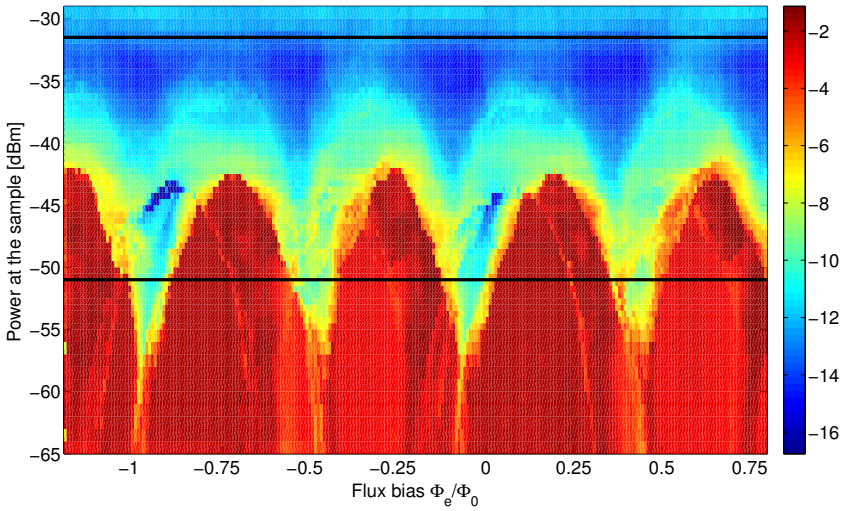

Figure 21: Input power at the sample vs. flux bias for a SQUID periodicity of 90μm. The color code indicates the depth of the dip [dB] (over the measured frequency interval) for each point in the power vs. flux bias plane (see text). The black horizontal lines enclose the power range, within which the change in depth of the dip in transmission over all flux bias values exceeds 5.25dB.

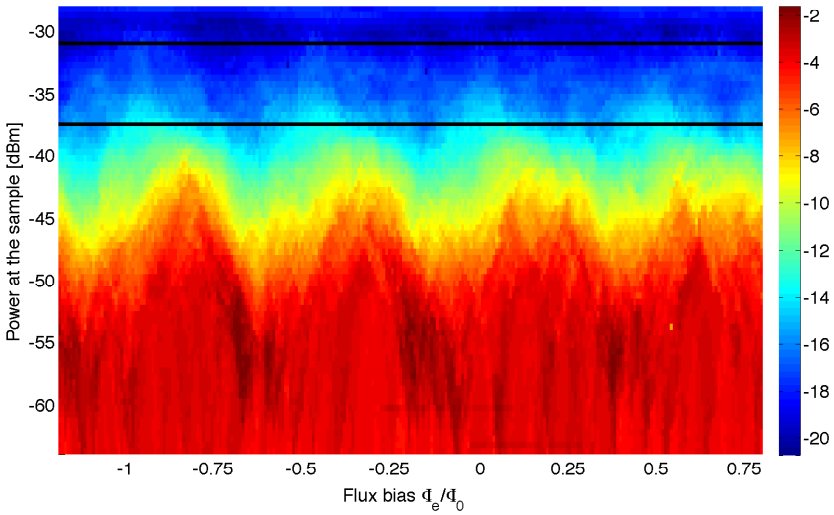

Figure 22: Input power at the sample vs. flux bias for a SQUID periodicity of 225μm. The color code indicates the depth of the dip [dB] (over the measured frequency interval) for each point in the power vs. flux bias plane (see text). The black horizontal lines enclose the power range, within which the change in depth of the dip in transmission over all flux bias values exceeds 5.25dB.

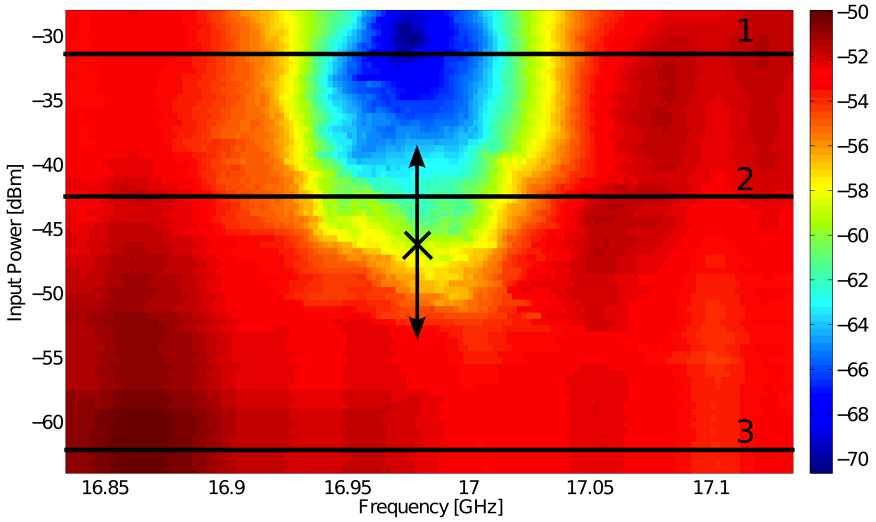

Figure 23: Change of dip position with changing flux (indicated by arrows) in input power vs. frequency diagram.

3.6.1 Occurrence of 2-dips-per-Φ_0 phenomenon

The transmission of the microwaves along the CPTL depends on the externally applied flux as is discussed in more detail in section 3.5.
The power vs. flux bias diagrams (figures 20, 21 and 22) reveal that one period Φ_0 contains two areas of high (and low) transmission for the intermediate power values. Thus, increasing the flux through the SQUID from $\Phi = 0$ to $\Phi = \Phi_0$ causes two "peaks". From the measurement results illustrated in figures 20, 21 and 22 we extract a period of $\Delta I_b = 2.5 \cdot 10^{-5}$A. This value fits very well with our theoretically expected value $I_b = 2.5 \cdot 10^{-5}$A from chapter 3.4.

Experimentally the assumption that two peaks form one period is reinforced by the observation that e.g. in figure 20 the pattern alternately consists of a narrow and a wide peak. This periodicity can also be seen in figure 21 where every other peak is very wide at low power values. The pattern of two peaks for every one flux quantum also fits with figure 22 although here the structure is less sharp.

An explanation of this 2-dips-per-Φ_0 phenomenon can be given as follows.
In figure 24 we plotted $f_{res} = \frac{1}{2\pi\sqrt{L_{tot}(\Phi)C}}$ with L_{tot} from equation (12) against the normalized external flux $\frac{\Phi_e}{\Phi_0}$.The resonance frequency of our SQUID transmission line is about 17GHz. The theoretical curve of f_{res} vs. Φ_e in figure 24 shows that this resonance frequency is excited at two different values for Φ_e within each period $\Phi_e \in [0, \Phi_0]$. Therefore it is clear that every two dips in the transmission represent a period of one flux quantum Φ_0 in the external flux that goes through the SQUID loop.

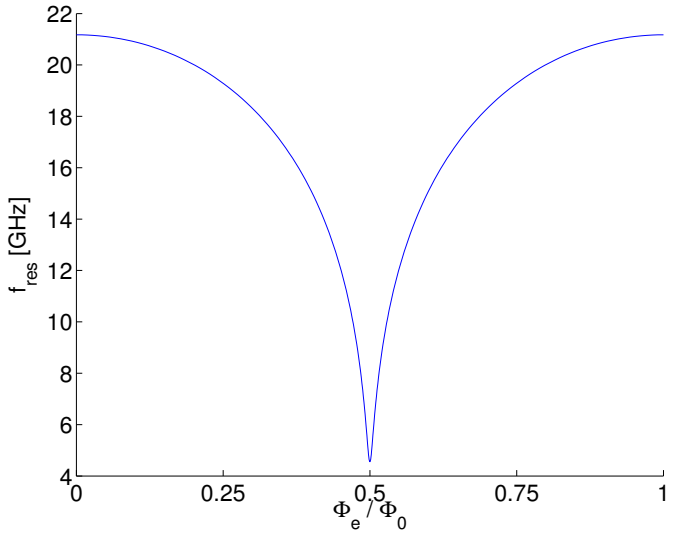

Figure 24: SQUID resonance frequency depending on the external flux.

3.6.2 Power range of flux dependence

Important for our investigations is the power range, in figures 20, 21 and 22, in which the depth of the dip in transmission changes with the parameter Φ_e. This work is focussed mainly on investigating a potential dependence of this range on the period of the SQUIDs in the array.

For investigating the potential dependence, a limit value (i.e. the level of change in depth of the dip in transmission) was defined, which had to be exceeded by the difference between maximal and minimal depth of the dip in transmission as explained in detail in chapter 3.6. The behavior is flux dependent at a certain power if the limit value is exceeded there.
Values for the power range, i.e. the differences between the respective first and last power at which the limit value is exceeded are enlisted in table 3 for different limit values. The limit values are chosen as absolute values. The limit values cover the complete range of power differences in which all three curves exist, as depicted in figure 25.

Table 3: Power range [dB] of flux dependence depending on distance and absolute limits of change in depth of the dip in transmission that is to be exceeded

	distance d [μm]		
absolute limit [dB]	55	90	225
5.00	**19.0**	19.5	6.5
5.25	16.5	19.5	6.5
5.50	16.0	16.5	6.5
5.75	16.0	16.5	0.5
6.00	16.0	15.5	0.5

For calculating the numbers for $d = 225\mu$m an error in measurement was dismissed. This is explained in further detail in the description of figure 25.

For the distance 90μm and the absolute limit 5.25dB there is the value 19.5dB in table 3. This means that the black bars in figure 21 should be 19.5dB apart. This is indeed the case. This means that the power range, in which the transmission is to be called flux dependent, is 19.5dB wide for the limit value 5.25dB. Therefore the depth of the dip in transmission changes, over a power range of 19.5dB, more than 5.25dB, when the external flux bias is changed over the measured interval.

Calculating the bold numbers (in table 3 and 4) at least one of the analogous bars to the black bars in the three figures (20, 21 and 22) above was at the first or last power that was measured. Therefore the actual numbers might be larger than stated.

The resulting power ranges in table 3 indicate that for each fixed limit value the power range of flux dependence increases in the step from $d = 55\mu$m to $d = 90\mu$m and decreases from $d = 90\mu$m to $d = 225\mu$m to a level below that of $d = 55\mu$m. The only exception is the limit value 6dB for which the power range decreases in both steps.

Another way of performing this analysis is by comparing relative limit values instead of absolute values. For calculating a relative value a reference value is needed. As such the maximal depth of the dip in transmission for each SQUID periodicity is chosen respectively. The maximal depth of the dip in transmission used in table 4 are the lowest transmission values indicated respectively in the color bars in figures 20, 21 and 22. These values are: $d = 55\mu\text{m} : -19\text{dB}$, $d = 90\mu\text{m} : -14\text{dB}$, $d = 225\mu\text{m} : -18\text{dB}$.
The relative limit was then calculated via

$$\text{limit}_{\text{relative}} = \left| \frac{\text{limit}_{\text{absolute}}}{\text{maximal depth of dip}} \right|. \tag{37}$$

The results of this analysis are seen in table 4. The pattern observed now is again an increase in power range of flux dependence from $d = 55\mu$m to $d = 90\mu$m and a decrease from $d = 90\mu$m to $d = 225\mu$m to a level below that of $d = 55\mu$m.
This relative way of illustration is probably more meaningful because the normalization with respect to the maximal depth of the dip in transmission makes the results better fit for comparison. The overall pattern, however, is the same in tables 3 and 4. They both indicate that no consistent behavior can be observed. A possible explanation for these findings is that there might be two effects, a short-ranging and a longer-ranging effect, that could have an impact. We definitely have to take into account our considerations in section 2.3, where we found that the SQUIDs in the array with the periodicity $d = 225\mu$m are not exposed to a magnetic field that is similar enough for all SQUIDs to be driven by a similar force. Furthermore, we found in section 3.3 that the current induced in a SQUID by another SQUID is negligibly small for $d = 225\mu$m and also for $d = 90\mu$m. Therefore there cannot be much coupling between them.

Table 4: Power range [dB] of flux dependence depending on distance and relative limits of change in depth of the dip in transmission that is to be exceeded

	distance d [μm]		
relative limit	55	90	225
20%	**23.0**	31.0	19.0
25%	**20.0**	29.5	8.5
30%	16.0	25.0	6.5
35%	8.5	19.5	0.0
40%	8.0	16.5	0.0

For calculating the numbers for $d = 225\mu$m the same error in measurement as above was dismissed.

Another possibility to illustrate the data even more clearly will be described in the following. Figure 25 shows the change in depth of the dip in transmission (over the measured flux bias interval) on the vertical axis. On the horizontal axis the input power at the VNA is plotted. This is an analogous illustration to the ones in figures 20, 21 and 22, but reduced by one dimension, the flux bias. In each of these three figures two horizontal lines are drawn representing the first and last power at which a power difference of 5.25dB is exceeded over all frequencies and flux bias values.
To get the equivalent information from figure 25 a horizontal line has to be drawn at the desired change in depth of the dip in transmission (vertical axis). The difference of the input power values (horizontal axis) of the intersection points then give the power range of flux dependence exceeding the specified change in depth of the dip in transmission.

When looking at the data for $d = 90\mu$m in figure 25 the highest values of power difference are probably due to a measurement error. Evidence for this assumption can be seen in figure 21. Around the power values at the sample of about -42dBm to about -48dBm there are two dark blue areas. These indicate a much lower transmission than expected. Therefore the peak in figure 25 should actually be lower between -42dBm and -48dBm.

The curve for $d = 55\mu$m shows a relatively flat plateau with a little drop in the middle. Its noise level is relatively high, as was already shown in figure 20, compared to the other two

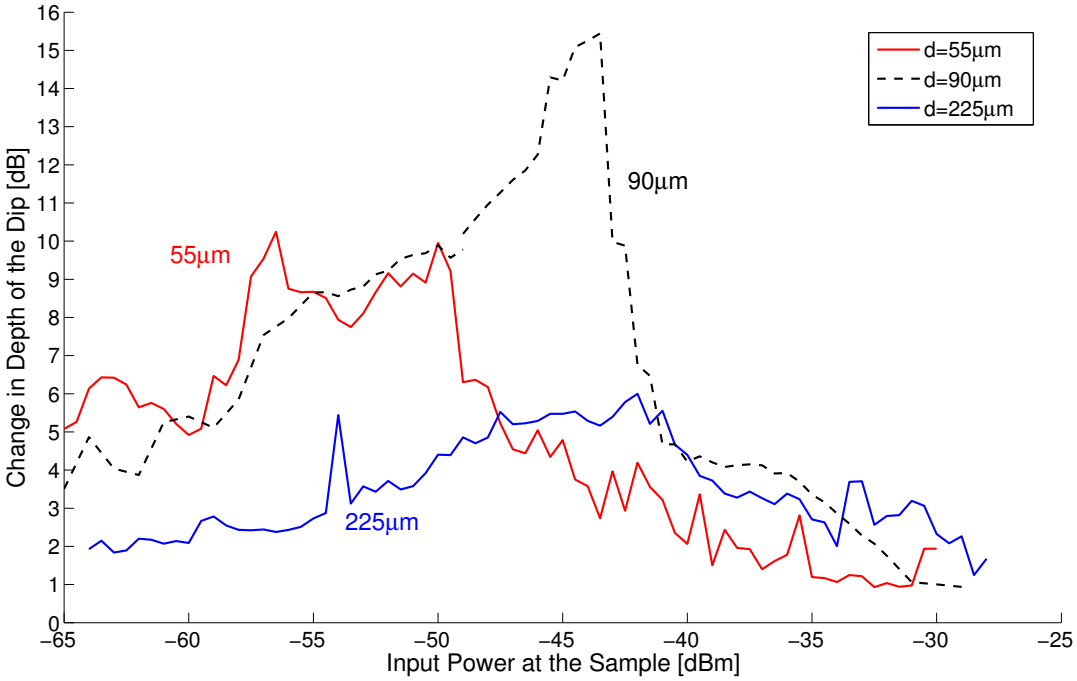

Figure 25: Change in depth of the dip in transmission (over the measured flux bias interval) versus input power at the sample.

curves.
The curves for $d = 225\mu$m and $d = 90\mu$m are shifted more towards higher input power values.
The sharp peak for $d = 225\mu$m at a power at the sample of about -54dBm can be dismissed as an error in measurement, too. It corresponds to the yellow area in figure 22 at an input power of about -54dBm.

Figure 25 shows no obvious correlation between the change in depth of the dip in transmission and the distance of the SQUIDs.

4 Conclusion and Outlook

In this thesis the effect of a linear rf-SQUID array on the transmission of a microwave, through a coplanar transmission line (CPTL), was investigated. The potential correlation between the periodicity of rf-SQUIDs and the power range in which the transmission of the microwave signal depends on the flux threading the SQUIDs was examined.

The CPTL and the SQUID arrays were fabricated of niobium on a Si-substrate. A SQUID array was placed in the gap on either side between the central line and the ground planes of the CPTL.
The chip, with the structures on it, was installed in a cryostat at liquid helium temperature. The microwave signal was supplied by a Vector Network Analyzer. The transmission was measured for three different periodicities of the SQUIDs (55μm, 90μm and 225μm). We varied the following variables: input power and frequency of the microwave signal and the external flux bias.
For each pair of input power and flux bias values our Vector Network Analyzer (VNA) sent a frequency sweep through the central line on the chip.

In our measurements we found the transmission of the microwaves through the CPTL to be dependent on the externally applied flux bias and the frequency of the microwave signal.
It depends on the flux bias because the SQUIDs can be considered as LC oscillators in which the amplitude of the induced current depends on the flux through the loop, according to the first Josephson relation. Due to the oscillatory nature of the magnetic field of the microwave signal the average external magnetic field at the sample was given only by the magnetic field due to the coil. The magnetic field of the coil penetrated the SQUIDs perpendicularly.
A periodic behavior of the transmission regarding the external flux from the coil was found for all three SQUID arrays with different periodicities. The bias current in the coil was chosen over such a range that in total two magnetic flux quanta threaded the SQUID loops. The power vs. flux bias diagrams reveal that for each Φ_0 in external flux bias threading the loop there are two maxima and two minima in transmission.
The transmission also depends on the frequency of the microwave signal because the amplitude of driven oscillations, in general, is greatest if the oscillator is driven at its resonance frequency. The resonance frequency of our SQUIDs is about 17GHz.
The microwaves provided the alternating magnetic field, around the central line, which drove the current oscillations in the SQUIDs. Thus they supplied the energy for driving the oscillations and they significantly lost energy if the induced current had a large amplitude.

The transmission, however, was affected by the external flux from the central line only in a certain range of input power values.
For input power values very high or very low in our measurements there was no dependence on the external flux. But there was an intermediate power range in which the transmission depended on the external flux of the coil. We substantiated this finding by comparing it to the results of a simulation.

According to our measurements there is no consistent correlation between the power range, in which the transmission of a microwave signal is flux dependent, and the distance between the SQUIDs.

The SQUIDs couple magnetoinductively with each other. The current induced in a SQUID either by another SQUID or by the CPTL was calculated using the concepts of mutual inductance and coupling coefficient. It was found that the current induced by another SQUID is small compared to the current induced by the CPTL. Our calculations showed that in the case of the smallest periodicity between the SQUIDs (55μm) the induced current by another SQUID is about 70 times smaller than the current induced by the CPTL. This was calculated using the maximal current $I_c = 5\mu$A in the other SQUID and a typical microwave power of $P = -50$dBm through the CPTL. This suggests that the effect of coupling SQUIDs is small even for those with the largest mutual inductance between them. For larger periodicities (90μm and 225μm) the induced current is even orders of magnitude smaller.
Furthermore the SQUIDs in the array with the periodicity 225μm were not exposed to a similar magnetic field over the whole array. Thus, they were not driven by the same force.

We propose to repeat the measurements with some alterations.
For one, the amplifier used was at room temperature. With an amplifier inside the cryostat lower input power values can be used.
Furthermore SQUID arrays with smaller periodicities should be used to increase the coupling effect of the SQUIDs among each other.
For further calculations it is to be noted that the coupling coefficient $\widetilde{F}$ was derived in reference [6] for a setup that does not fully match our setup with the CPTL.

5 References

[1] Vadim V. Schmidt, *The physics of superconductors: Introduction to Fundamentals and Applications*, Springer-Verlag, Berlin, 1997

[2] Susanne Butz, *Experiments on Asymmetric dc-SQUIDs: Searching for the Münchhausen Effect*, Diploma thesis, 2010

[3] John Clarke and Alex I. Braginski, *The SQUID Handbook Vol. I: Fundamentals and Technology of SQUIDs and SQUID Systems, Wiley-VCH, 2004*

[4] Konstantin K. Likharev, *Dynamics of Josephson Junctions and Circuits*, Gordon and Breach Science Publishers, New York, 1986.

[5] Steve M. Anlage, *The physics and applications of superconducting metamaterials*, Journal of Optics, **13** (2011), no. 2

[6] N. Lazarides and G. P. Tsironis, *rf superconducting quantum interference device metamaterials*, Appl. Phys. Lett. **90** (2007), no. 16

[7] N. Lazarides, G. P. Tsironis and M. Eleftheriou, *Dissipative Discrete Breathers in rf SQUID Metamaterials*, Nonlinear Phenomena in Complex Systems, vol. **11** (2008) , no. 2

[8] Reinmut K. Hoffmann, *Integrierte Mikrowellenschaltungen: Elektrische Grundlagen, Dimensionierung, technische Ausführung, Technologien*, Springer-Verlag, Berlin, 1983

[9] Susanne Butz, private communication

[10] Simulation calculated by Sergey V. Shitov

[11] Michael Tinkham, *Introduction to superconductivity*, 2. ed. ed., Dover Publ., Mineola, NY, 2004.

[12] Wolfgang Demtröder, *Experimentalphysik 2: Elektrizität und Optik*, Springer-Verlag, Berlin, 2009

Hiermit versichere ich, dass ich die Arbeit selbstständig verfasst habe und keine anderen als die angegebenen Quellen und Hilfsmittel benutzt habe, die wörtlich oder inhaltlich übernommenen Stellen als solche kenntlich gemacht und die Satzung des KIT zur Sicherung guter wissenschaftlicher Praxis in der gültigen Fassung beachtet habe.

6 Acknowledgements

I want to thank Professor Alexey Ustinov for providing me the opportunity to work on this interesting project. I learned a lot about superconductivity and SQUID physics.
I also want to thank my tutor Susanne Butz for very patiently supporting me during the measurements and the analysis of the gathered data. Her answers to all of my many questions really helped me a lot. I could not have had a more supportive tutor.
I am also grateful for all the explanations Philipp Jung gave me regarding network analysis, measurement technique and many other topics.
Furthermore I want to thank Philipp and Susanne for permitting me to use the chip samples they had designed.